



Caesium Salt of Tungstophosphoric Acid Supported on Mesoporous SBA-15 Catalyst for Selective Esterification of Lauric Acid with Glycerol to Monolaurin

Syamima Nasrin Mohamed Saleh¹ · Mohd Hizami Mohd Yusoff¹ · Ahmad Zuhairi Abdullah¹

Received: 12 July 2017 / Accepted: 3 December 2017 / Published online: 11 December 2017
© King Fahd University of Petroleum & Minerals 2017

Abstract

Cs_{2.5}H_{0.5}PW₁₂O₄₀ supported on SBA-15 catalysts were prepared via two-sequential-step post-impregnation method with different ratios of cesium salt. The synthesized catalysts were then characterized using nitrogen adsorption–desorption, FTIR, EDX, SEM, BET and TGA analyses in order to determine the physicochemical properties of the catalysts. The activity of the catalysts in the esterification of glycerol to monolaurin was investigated under various reaction parameters including catalyst loadings, reaction temperatures and glycerol-to-lauric acid molar ratio. The highest lauric acid conversion (71.8%) with 44.9% of monolaurin yield was obtained using 20 wt% Cs-HPW/SBA-15 catalyst in 4 h at 170 °C using 4:1 of glycerol-to-lauric acid molar ratio and 2.5 wt% of catalyst loading. This catalyst was stable and reusable for up to three cycles in the esterification reaction without significant loss in catalytic activity.

Keywords 12-Tungstophosphoric acid · SBA-15 · Selective esterification · Lauric acid · Monolaurin

1 Introduction

Recently, functionalized mesoporous silicas have attracted considerable interest in the production of monoglycerides due to their uniform and large pore sizes which are advantageous in facilitating the reaction involving bulky reactants. Several attempts have been made on the functionalization of SBA-15 with various active species to increase the catalytic activity toward high monoglyceride selectivity. Other than sulfated zirconia [1] and propyl sulfonic acid [2,3] as active species, heteropolyacid (HPA) also has the potential for such reaction. In a recent study, Simsek et al. [4] found that STA/SBA-15 catalyst exhibited high monolaurin selectivity within 3 h of reaction but as the reaction prolonged, the selectivity was found to decrease. Meanwhile, Hoo et al. [5] synthesized 12-tungstophosphoric acid (HPW) supported on SBA-15 catalyst for selective esterification of lauric acid with glycerol to monolaurin. After 6 h, the catalyst with 20 wt% HPW loading exhibited the highest shape selective

effect with 70% of lauric acid conversion and 50% of monolaurin yield. However, the thermal stability and reusability of the catalyst were not explored.

Despite its good catalytic activity, leaching of the active sites from the SBA-15 during the reaction has become the major concern for this catalyst. Thus, it becomes a challenge to create a practical, durable and highly reactive catalyst, which needs further modifications for the acidic site of the catalyst. This can be done by introducing the caesium (Cs) salts of tungstophosphoric acid (Cs-HPW) onto SBA-15. Cs-HPW is known for being highly acidic and has unique physical characteristics and good activity for various organic reactions [6]. Therefore, by impregnating the Cs-HPW salt on the mesoporous SBA-15 support, the thermal stability and the surface acidity of the catalyst should be improved as well. Previously, Dias et al. [6] proved that the acidity was increased sharply as the Cs content increased and all Cs derivatives of HPW revealed both Brønsted and hydrogen-bonded sites in the structure. Madhusudhan et al. [7] prepared Cs salts of HPW deposited on SBA-15 and the catalyst showed considerably good performance in acidic reactions (propionylation and alkylation). In another study, Landau et al. [8] also found that Cs salt of HPW dispersed on SBA-15 showed rather improved performance toward NO_x storage. Although Cs salts of HPAs have shown good performances

✉ Ahmad Zuhairi Abdullah
chzuhairi@usm.my

¹ School of Chemical Engineering, Engineering Campus,
Universiti Sains Malaysia, 14300 Nibong Tebal, Penang,
Malaysia

in various types of reactions, no work has been reported so far on the use of Cs salts of HPW supported on SBA-15 in selective esterification of lauric acid with glycerol to monolaurin.

In the present work, Cs-HPW acidic salt supported on SBA-15 catalysts has been synthesized and used in the esterification of glycerol with lauric acid to monolaurin. Particular attention has been given to the shape selective effect and stability of the catalyst for this particular reaction. Correlation between the catalyst characteristics and the catalytic behavior has been established in order to demonstrate the effect of its intrinsic properties on the activity. In addition, effects of process variables such as catalyst loading, reaction temperature and glycerol-to-lauric acid molar ratio have been investigated to gain better understanding of the glycerol esterification reaction toward the production of monolaurin. The spent catalyst has also been studied to investigate the stability of the morphological and chemical properties of the catalyst after three consecutive runs.

2 Experimental

2.1 Synthesis of Cs-HPW/SBA-15 Catalysts

The Cs-HPW/SBA-15 catalysts were synthesized via two-sequential-step post-impregnation and incipient wetness technique [9]. The parent SBA-15 was prepared following a method described in the literature [10]. 4 g of Pluronic P123 was dissolved in a solution containing 125 ml of 1.9 M HCl. The solution was stirred at 40 °C for 2 h, and 8 g of tetraethyl orthosilicate (TEOS) was slowly added into the mixture under a vigorous stirring at 40 °C for 22 h. The solution was then transferred into a Teflon bottle and left for another 24 h at 100 °C. The solid product was then filtered, washed with deionized water and dried at room temperature for 24 h which was then followed by calcination in air at 500 °C for 6 h. For the preparation of 10 wt%Cs-HPW/SBA-15 catalyst, 0.0304 g of CsNO₃ was dissolved in 10 mL of water. Then, 1 ml of the solution was added every 2 min to the SBA-15 under a constant stirring. The formed paste was then stirred for 20 min until the free-flowing powder was formed. The resulted material was dried at 100 °C for 4 h to remove the remaining solvents and subjected to calcination at 300 °C for 4 h. The obtained product was then impregnated using 0.1795 g of 12-tungstophosphoric acid (HPW) in 10 ml of ethanol. The resulted product was dried in an oven at 100 °C for 4 h and then calcined at 300 °C for another 4 h. For a variation of Cs-HPW concentration (20, 30 and 40 wt%), the catalysts were synthesized as discussed earlier with the appropriate amount of Cs-HPW and their corresponding loadings are denoted as *x*Cs-HPW/SBA-15; *x* stands for the wt% of Cs-HPW. For comparison, HPW/SBA-15 catalyst was synthesized via

impregnation method [11]. In a typical synthesis, 0.4 g of 12-tungstophosphoric acid (HPW) was dissolved in 10 ml of ethanol and the mixture was added into 1.6 g of SBA-15. Then, the resultant product was dried at 60 °C for 12 h and then followed by another 12 h at 100 °C.

2.2 Characterization of the Catalysts

SBA-15, HPW/SBA-15, and Cs-HPW/SBA-15 catalysts with different loadings were characterized using various techniques to study the physical, chemical and morphological properties of the catalysts. Nitrogen adsorption–desorption analysis was performed using a Quanta-chrome Autosorb 1C surface analyzer to investigate the surface characteristics of all synthesized catalysts. Fourier transform infrared spectroscopy (FTIR) analysis was conducted by means of a Shimadzu IR Prestige-21 system using the KBr pellet technique. Scanning electron microscopy (SEM) images were taken using a Quanta FEG 450 SEM, and energy-dispersive X-ray (EDX) analysis was also performed using the same equipment. Thermal gravimetric analysis (TGA) was carried out on a PerkinElmer (TAC 7/DX). The analysis was carried out by raising the temperature from 0 to 900 °C at a ramping rate of 20 °C/min under 50 mL/min of O₂.

2.3 Catalytic Activity

The esterification reaction was carried out in a three-necked flask reactor equipped with a magnetic stirrer bar, a thermocouple, a sampling neck and a tube connected to a vacuum pump. In a typical procedure, lauric acid, glycerol and specified amount of catalyst were added into the reactor and heated to the desired temperature under a reduced pressure of 50.8 cmHg. Then, the mixture was stirred at 750 rpm for up to 6 h. The experimental conditions employed in this work are summarized in Table 1. After the reaction, the product samples were analyzed using a gas chromatograph (Agilent Technologies 7890A GC system) equipped with a CP-Sil 5CB (15 m × 0.32 mm × 0.1 mm) column. The lauric acid conversion and monolaurin selectivity were calculated according to the method proposed by Hermida et. al [2].

Table 1 Summary of experimental conditions

Variables	Value
Catalyst loadings (wt%)	10, 20, 30, 40
Catalyst concentration with respect to reactants (wt%)	1.5, 2.5, 3.5
Operating temperature (°C)	150, 160, 170
Glycerol/fatty acid molar ratio	2:1, 3:1, 4:1

3 Results and Discussion

3.1 Catalyst Characterization

3.1.1 Surface Analysis

The surface analysis results of the SBA-15, HPW/SBA-15, and Cs-HPW/SBA-15 catalysts with different loadings are represented in Table 2. Based on the results, it can be concluded that the synthesized SBA-15 having a surface area of 873 m²/g and average pore size of 61 Å is a mesoporous material. All catalysts had high specific total surface areas in the range of 383–671 m²/g. This finding indicated that all catalysts had a large interfacial surface of contact which allow the interaction between the reactants with the active sites. Nevertheless, there was a slight increase in the total surface area of the unmodified HPW/SBA-15 and 10 wt%Cs-HPW/SBA-15 in which it only increased from 630 to 671 m²/g. Niiyama et al. [12] reported that the addition of the second group of large metal ions like Cs⁺ (Cs salts of HPAs) on the SBA-15 could improve the specific surface area of the catalyst. However in this study, the increment was minimal so that it can be considered as negligible. This finding suggested that the pore structure of the catalysts remained intact despite the addition of Cs to indicate the stability of the porous structure.

Furthermore, the BET surface area for all Cs-HPW/SBA-15 catalysts decreased with increasing Cs-HPW loading. As the Cs-HPW loading on the SBA-15 support was increased from 10 to 40 wt%, the BET surface area decreased from 671 to 383 m²/g. This phenomenon is in agreement with a previously reported work [13]. Similar trend was also observed for the pore volume in which it decreased from 0.89 to 0.53 cm³/g. However, the pore volumes for 20 wt%Cs-HPW/SBA-15 and 30 wt%Cs-HPW/SBA-15 catalysts were found to be similar (0.75 cm³/g). At 30 wt% loading, the

Table 2 Surface characteristics of SBA-15, HPW/SBA-15 and Cs-HPW/SBA-15 catalysts with different Cs-HPW loading

Catalyst	Surface area (m ² /g)	Total pore volume (cm ³ /g)	Average pore size (Å)
SBA-15	873	0.99	61
HPW/SBA-15	630	0.84	61
10 wt%Cs-HPW/SBA-15	671	0.89	60
20 wt%Cs-HPW/SBA-15	556	0.75	58
30 wt%Cs-HPW/SBA-15	506	0.75	61
40 wt%Cs-HPW/SBA-15	383	0.53	59

deposition of active sites inside the pore could have reached its limit and as a result, the deposition mainly occurred on the outside of the pore structure. Nevertheless, this result indicated that the Cs-HPW was successfully introduced into the internal pores of the SBA-15. Meanwhile, all catalysts exhibited large pore sizes within the range of 58–61 Å. Although the difference can be considered as negligible, a slight increase in the pore size would give significant effect on the catalytic activity in terms of reactant's conversion and selectivity, as demonstrated in this work. For the reaction involving bulky reactants, pore size plays an important role in facilitating the interaction between the molecules with active sites within the pore. Small pore sizes could cause a geometrical constraint in accommodating the reactant molecules within the pores while larger pores will minimize diffusion limitations for bulkier molecules such as long-chain fatty acid.

The nitrogen adsorption–desorption isotherms of the SBA-15 support and the Cs-HPW/SBA-15 catalysts are shown in Fig. 1. All isotherms exhibited the typical type IV isotherm (according to the IUPAC classification) [11]. Furthermore, all isotherms exhibited the typical hysteresis loops of H1 at relative pressures between 0.4 and 0.9. The hysteresis type H1 isotherms with narrow pore size distributions are observed and this finding proved that the catalysts were porous materials with agglomerated or uniformly packed spheres and regular arrangement. Adsorption and desorption branches in the hysteresis curve formed are nearly parallel with SBA-15 to indicate the formation of the regularly shaped pores during the synthesis. Hence, the hysteresis curves in the multilayer ranges of physisorption, the isotherms were related with capillary condensation in the mesopores [2]. Besides, the sharp inflection on the adsorption branch of all the isotherms indicates that the catalysts have relatively high uniform mesopore sizes distribution.

Meanwhile, Fig. 2 shows the BJH pore size distribution of the support and catalysts. All catalysts showed narrow ranges of pore size distribution to prove the catalysts have regular and ordered pore structure [14]. As shown in Fig. 2, the SBA-15, 20 wt%Cs-HPW/SBA-15 and 40 wt%Cs-HPW/SBA-15 exhibited smaller peaks at lower pore sizes. This was attributed to the tensile strength effect possessed by the catalysts during the nitrogen adsorption–desorption [15,16]. The tensile strength hypothesis describes that at a certain pressure, a closure of the hysteresis loop will form due to the physical properties of the adsorption. It is basically because of the “ink-bottle-shape” of the pores and due to the small size of the pore throats [17]. As the name suggests, this type of pore opening which was narrower caused the absorbed N₂ to have some difficulty during the desorption process. This might be attributed to the uneven silica distribution and excessive silica at that particular region, forming silica plug [18].



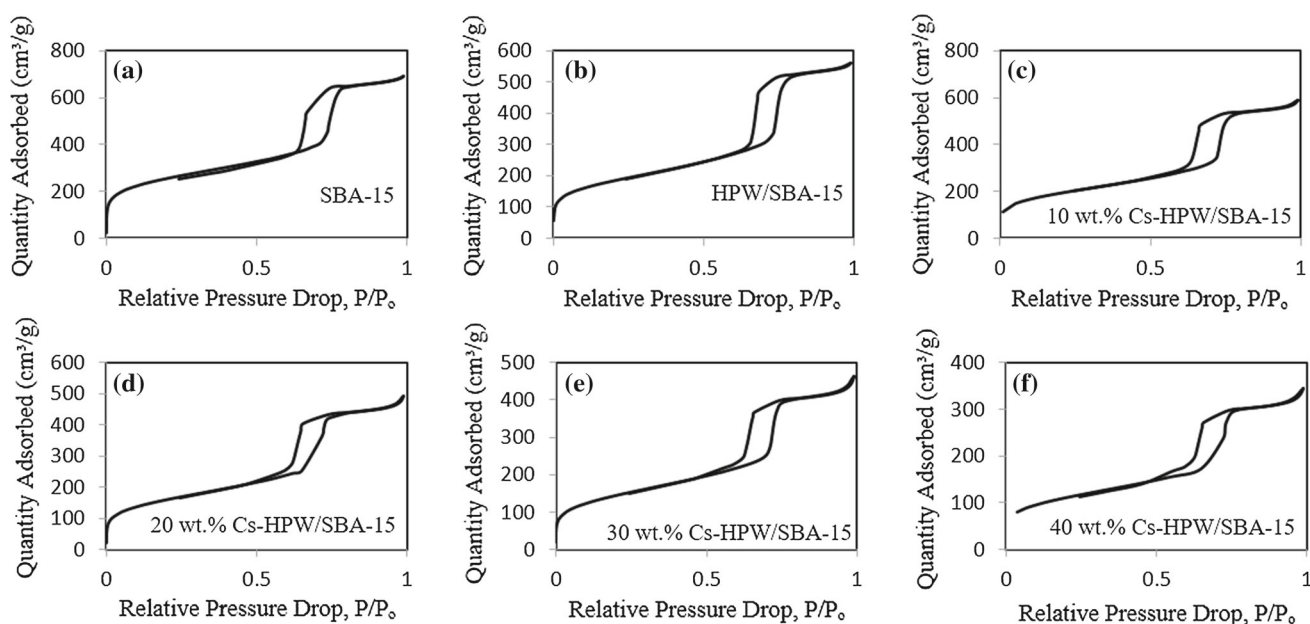


Fig. 1 Isotherm profiles of SBA-15, HPW/SBA-15 and Cs-HPW/SBA-15 catalysts with different Cs-HPW loading

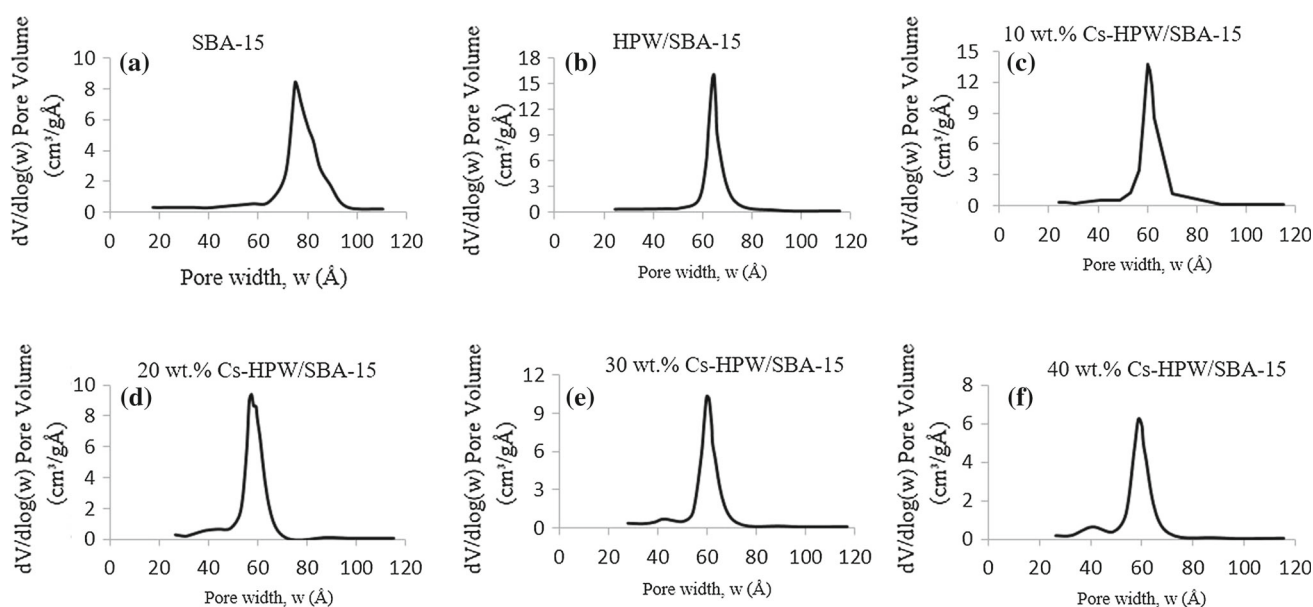


Fig. 2 BJH pore size distributions of SBA-15, HPW/SBA-15 and Cs-HPW/SBA-15 catalysts with different Cs-HPW loading

3.1.2 Fourier Transform Infrared Spectroscopy (FTIR)

Figure 3a shows the FTIR spectra for the SBA-15 support and the unmodified HPW/SBA-15 while Fig. 3b shows the FTIR spectra for all Cs-HPW/SBA-15 with different Cs-HPW loadings. The impregnation of Cs salts of HPW into the SBA-15 support evidently affected the structure of the catalysts due to partial or complete overlapping of bands of Cs-HPW supported on SBA-15 matrix. Bands between 800 and 1200 cm^{-1} are observed for all catalyst which can be represented by the presence of $\text{PW}_{12}\text{O}_{40}^{3-}$ Keggin ion

[2]. Meanwhile, the unmodified HPW/SBA-15 showed the spectrum containing the vibrations bands at 1082, 981, 897 and 803 cm^{-1} which could be correlated to the stretching vibrations of $\text{P}-\text{O}_a$, $\text{W}=\text{O}_d$, $\text{W}-\text{O}_b-\text{W}$ and $\text{W}-\text{O}_c-\text{W}$, respectively [19]. Furthermore, the complex Keggin structure was effectively preserved in all catalysts regardless of the different concentrations of Cs used in the preparation of catalysts. However, an overlapping was observed for the band corresponded to $\text{W}-\text{O}_b-\text{W}$ at 805–887 cm^{-1} in Fig. 3a with a strong absorption band of SBA-15 at 882 cm^{-1} in Fig. 3b. Basically, at lower loading, more homogeneous dis-

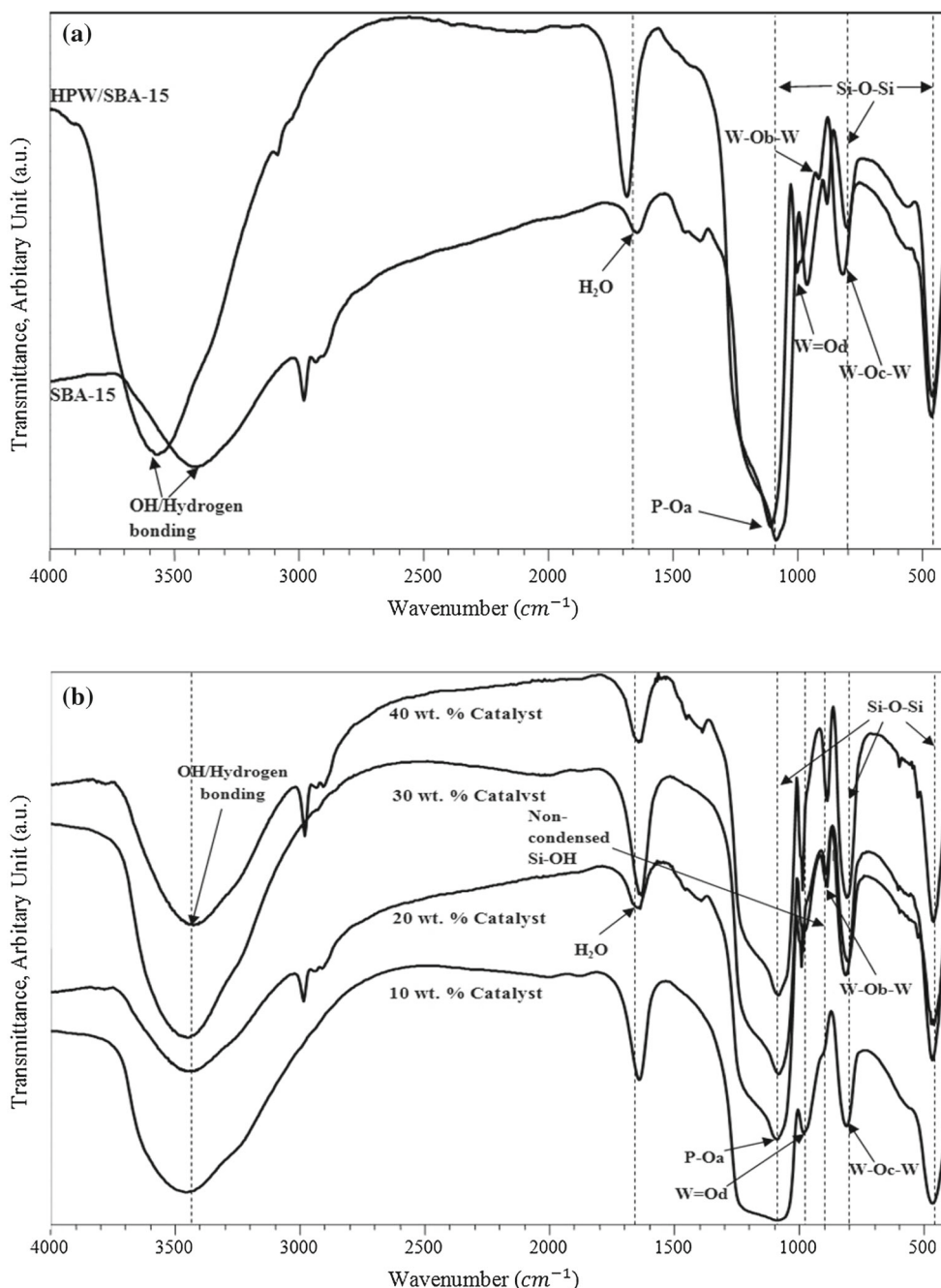


Fig. 3 a FTIR spectra of SBA-15 and HPW/SBA-15 and b FTIR spectra of Cs-HPW/SBA-15 catalysts with different Cs-HPW loading

persion of the active phase inside the pores of the SBA-15 support could be accomplished compared to the higher loadings.

Bands between 1082 to 462 cm^{-1} are observed which could be correlated to the Si-O-Si bond. Some of these bands are preserved in the synthesized catalysts. However, due to the strong absorption bands of silica from SBA-15, some of these bands are widened and partially overlapped. As shown in Fig. 3b, an asymmetric stretching of Si-O-Si at 1250–1083 cm^{-1} , a symmetric Si-O-Si

stretching at 805 cm^{-1} and a bending vibration of Si-O-Si at 459 cm^{-1} are observed to suggest the perseverance of the mesoporous structure of the SBA-15 support even at high Cs-HPW loadings. Bands are detected at 3451, 3447, 3452, 3440 cm^{-1} for 10, 20, 30 and 40 wt% of Cs-HPW loadings, respectively, and these bands are assigned to the Si-OH bonds that formed through the polar interactions between Si-OH water molecules. Other polar components such as hydrogen bond with the Si-

OH molecules could also cause the formation of this band [20,21].

Interestingly, all synthesized catalysts including SBA-15 support show an intense band at wavelengths of 1634–1640 cm^{-1} to represent the adsorbed water molecules. In general, the intensity of these bands was found to be higher for the Cs-HPW/SBA-15 catalysts as compared to the unmodified catalyst. This could be attributed to the presence of hydrophilic Si–OH groups in the support material, which could cause rapid adsorption of water molecules into the pores [5]. In addition, air humidity could also cause the phenomenon [22]. In fact, HPW itself is a hydrophilic molecule, and hence the SBA-15 supported Cs-HPW catalysts would definitely have a higher capability to absorb moisture or water molecules from the surrounding due to the availability of Si–OH bonds. At the wavelength between 1083 and 1085 cm^{-1} , a band is observed for all catalysts which could be assigned to $[\text{PW}_{11}\text{O}_{39}]^{7-}$ which usually presents at pH greater than 2. Upon modification of HPW by addition of Cs, the protons in HPW are actually replaced by the large cation in the Cs atom. The cation in Cs induces electrostatic anion–anion interactions in the catalyst [6]. Thus, the cation in Cs had replaced the proton in HPW and caused a decrease in the stretching frequencies or vibrations of all the bands, particularly at the bands representing the oxygen that was shared around the four edges.

3.1.3 SEM

Figure 4 shows the morphology of the SBA-15, HPW/SBA-15, and Cs-HPW/SBA-15 catalysts. As observed in the figure, all catalysts including the SBA-15 support exhibited well-ordered fibrous structures. All catalysts showed similarity in terms of the shape and surface morphology as compared to that of SBA-15 support (Fig. 4a). Hence, it proved that the catalysts were successfully synthesized and the desired shape, morphology and structure were successfully formed. The synthesized SBA-15 is composed of relatively uniform rope-like particles which are aggregated into fiber-like macroscopic structures. This morphology resembles the typical SBA-15 extended fiber-like structure [23] to indicate the successful synthesis of the SBA-15 mesopores.

There was no deposit on the surface of both HPW/SBA-15 (Fig. 4b) and the 20 wt%Cs-HPW/SBA-15 (Fig. 4d), and this was due to the flattening of the crystals. However, there are some traces of deposits on the external surface of 10 wt%Cs-HPW/SBA-15 (Fig. 4c). This could be attributed to the improper mixing of Cs salt with HPW, which in turn reduced the capability of impregnation of the Cs-HPW into the pores of the SBA-15 support leaving out tiny crystals on the surface. At Cs-HPW loadings of 30 and 40 wt%, crystals were deposited on the external surface of the SBA-15 support, as shown by the arrow in Fig. 4e and f, respectively. There is a greater tendency for clusters of crystals and deposits to form on the external surfaces of the support at high loadings

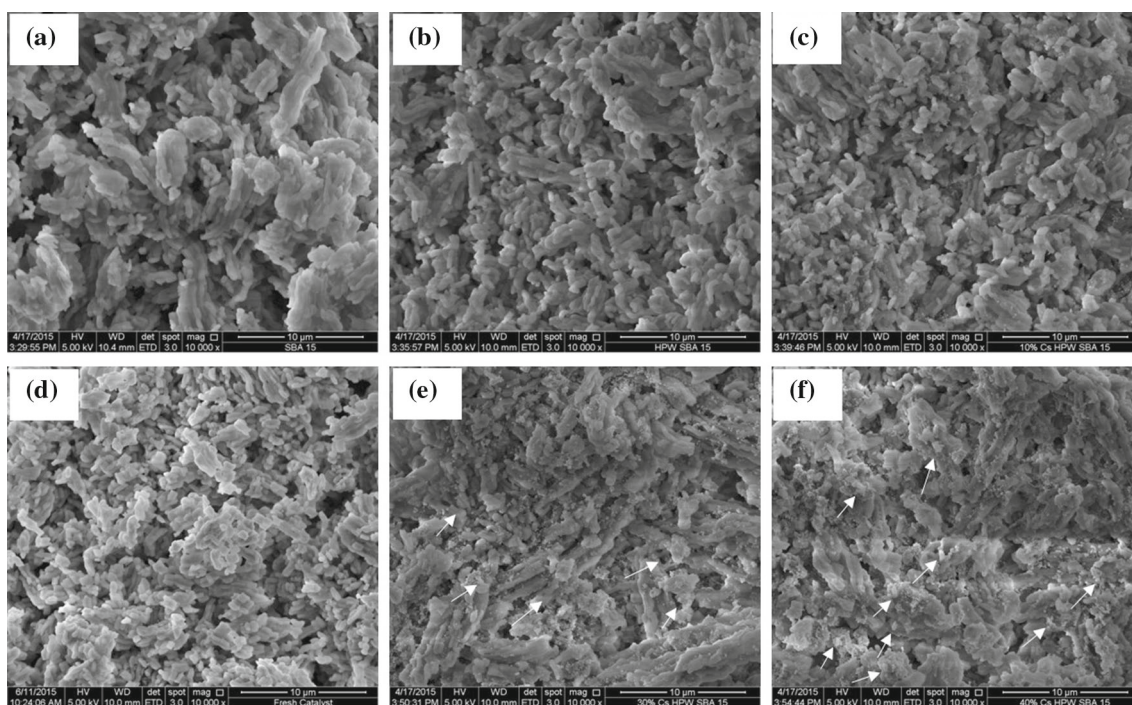


Fig. 4 SEM images for **a** SBA-15, **b** 20 wt%HPW/SBA-15, **c** 10 wt%Cs-HPW/SBA-15, **d** 20 wt%Cs-HPW/SBA-15, **e** 30 wt%Cs-HPW/SBA-15, **f** 40 wt%Cs-HPW/SBA-15 samples (magnification 10kX)



(30 and 40 wt%) in post-impregnation method [24]. Higher catalyst loading means that more active phases are available to accommodate the pores of the support, resulted in most of the pores being occupied. This would result in the crystallization of some of the anions (especially the oxidized form of HPW) on the external surfaces. This finding also indicated that the HPW anions were not fully impregnated into the mesopores due to the size restriction of the SBA-15 and the accumulation of the excess HPW anions on the external surfaces of the support.

3.1.4 EDX Analysis

The chemical composition of silicon (Si), oxygen (O), tungsten (W) and caesium (Cs) elements was detected via EDX analysis, and the results are tabulated in Table 3. In actuality, the catalyst employed in this study consisted of $Cs_{2.5}H_{0.5}PW_{12}O_{40}$, with the enclosure of the anions in between the Si layers. However, the phosphorus (P) was not detected in all the synthesized catalysts. The element might be fully entrapped in the internal pores rather than on the external surface of the catalyst. Moreover, the amount of P in the total catalyst weight could be extremely low to be detected via EDX analysis. Thus, the actual amount of Cs-HPW loading on the support could not be estimated due to the absence of P. Furthermore, the amount of O was overlapped in both HPW anion and SBA-15 support, making it impossible to distinguish the amount of O present merely in the Cs-HPW anion. Nevertheless, the difference between the designated Cs-HPW loadings from the detected one was 1.71, 0.19, 1.61, 1.74 and 1.51 wt% for HPW/SBA-15, 10, 20, 30 and 40 wt%Cs-HPW/SBA-15, respectively. Thus, it proved that the incorporation of Cs into HPW with SBA-15 was a success since the error detected was sufficiently less than 8%. The missing percentage of Cs-HPW was attributed to the missing P element.

As expected, the difference between the designated Cs-HPW loadings from the detected results increased at higher loading. This might be due to the evenly dispersed Cs-HPW

anions in the mixture of Cs-HPW/SBA-15 catalysts as the amount of anions increased at higher loadings. Higher dispersion in the mixture would result in the better permeation of the Cs-HPW anions into the internal pores of the catalyst. Furthermore, the W element also increased with increasing Cs-HPW loadings. This was mainly contributed by the presence of higher amount of Cs-HPW anions at higher loadings, which eventually increased the possibility of tungsten trioxide (WO_3) formation on the surfaces.

3.1.5 Thermal Gravimetric Analysis (TGA)

Figure 5 shows the TGA analysis of the catalysts and HPW/SBA-15. The profiles show three stages of weight loss when it was heated to 900 °C and these regions could be assigned to the water elimination (region i), decomposition of the anhydrous samples by constitutive water removal (region ii) and crystallization process of constitutive oxides for the synthesized catalysts (region iii).

At the temperature around 29 to 105 °C (region i), a drastic weight loss was observed for all catalysts including HPW/SBA-15. This was mainly due to the loss of water by evaporation process accompanied by the crystallization process of the Cs-HPW/SBA-15 catalysts. It could also be observed that the weight loss of the catalysts increased in a sequence of 40 wt%Cs-HPW/SBA-15 (4.5 wt%), 30 wt%Cs-HPW/SBA-15 (5.0 wt%), 20 wt%Cs-HPW/SBA-15 (6.2 wt%), HPW/SBA-15 (9.0 wt%) and 10 wt%Cs-HPW/SBA-15 (12.4 wt%). At lower Cs-HPW loadings, the catalysts tend to be more hydrophilic due to the availability of the vacant sites in between the Si-OH bonds in the SBA-15. Hence, more water molecules were adsorbed and stored during the synthesis process, and upon heating, the water molecules would be evaporated, resulting in very significant weight losses. Meanwhile, at higher loadings of 30 and 40 wt%, more tungsten trioxide (WO_3) formed on the external surface of the SBA-15 support and WO_3 could have

Table 3 Results of EDX analysis on the SBA-15, HPW/SBA-15 and Cs-HPW/SBA-15 catalysts with different Cs-HPW loading

Catalyst	Component			
	O (wt%)	Si (wt%)	W (wt%)	Cs (wt%)
SBA-15	57.68	42.32	0.00	0.00
HPW/SBA-15	57.78	23.93	18.29	0.00
10 wt%Cs-HPW/SBA-15	54.50	35.69	8.93	0.88
20 wt%Cs-HPW/SBA-15	50.90	30.70	17.04	1.35
30 wt%Cs-HPW/SBA-15	48.83	22.91	25.85	2.41
40 wt%Cs-HPW/SBA-15	37.49	24.03	35.56	2.92

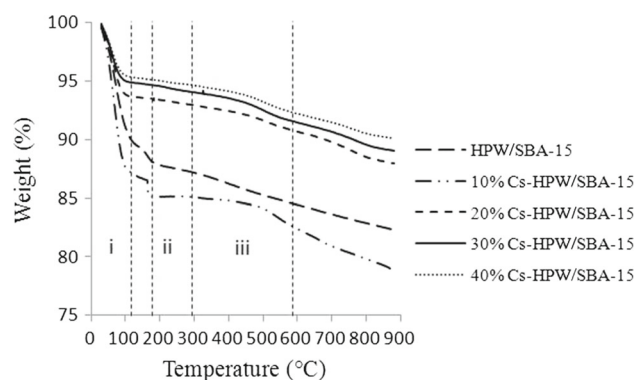


Fig. 5 TGA profiles of HPW/SBA-15, 10 wt%Cs-HPW/SBA-15, 20 wt%Cs-HPW/SBA-15, 30 wt%Cs-HPW/SBA-15 and 40 wt%Cs-HPW/SBA-15 catalysts

hindered the absorption of water during the synthesis process [21].

The second weight loss appears between 180 and 290 °C (region ii). In this region, the catalysts basically faced the removal of the remaining water molecules from the Cs-HPW/SBA-15 catalysts. The loss of water molecules actually allowed the crystallization of HPW to eventually form HPW Keggin ions. Traces of organic compounds such as P-123 during the preparation of the SBA-15 were removed in this region [25]. The third weight loss was observed between 290 to 590 °C whereby gradual weight losses were encountered by all the synthesized catalysts. This finding indicated the removal of the constitutional water that was formed from acidic protons and oxygen belonging to the Keggin units from the internal pores [11]. Dehydroxylation of silanol groups in the pure HPW usually occurs at a temperature of 485 °C [26]. Since all the synthesized catalysts did not undergo severe weight losses, it indicated that all synthesized catalysts were thermally stable without significant decomposition of acid sites below 900 °C. Still, they were reasonably thermally stable up to 200 °C and as these catalysts were not designated to be used at a temperature higher than that, the stability up

to that temperature would be sufficient. Hence, it could be concluded that the losses in weight of all the synthesized catalysts beyond this temperature could be attributed by the decomposition of the catalysts themselves. In brief, HPW anions of all the synthesized catalysts did not undergo severe decomposition. Hence, Cs-HPW/SBA-15 could be considered as a very thermally stable catalyst.

3.2 Catalytic Performance

3.2.1 Effect of Cs-HPW Loading on SBA-15 Support

Figure 6 shows the lauric acid conversion and monolaurin yield profiles of all Cs-HPW/SBA-15 and HPW/SBA-15 catalysts. As shown in Fig. 6a, an increase in the Cs-HPW loading significantly increased the conversion of lauric acid. After 6 h of reaction, 40 wt% catalyst shows the highest conversion which was then followed by 30, 20 and 10 wt% Cs-HPW/SBA-15 catalysts. This basically fits the theory very well that catalysts with higher active acidic sites should have higher activity. These results also suggested that at higher Cs-HPW loading (30 and 40 wt%), the catalysts might have

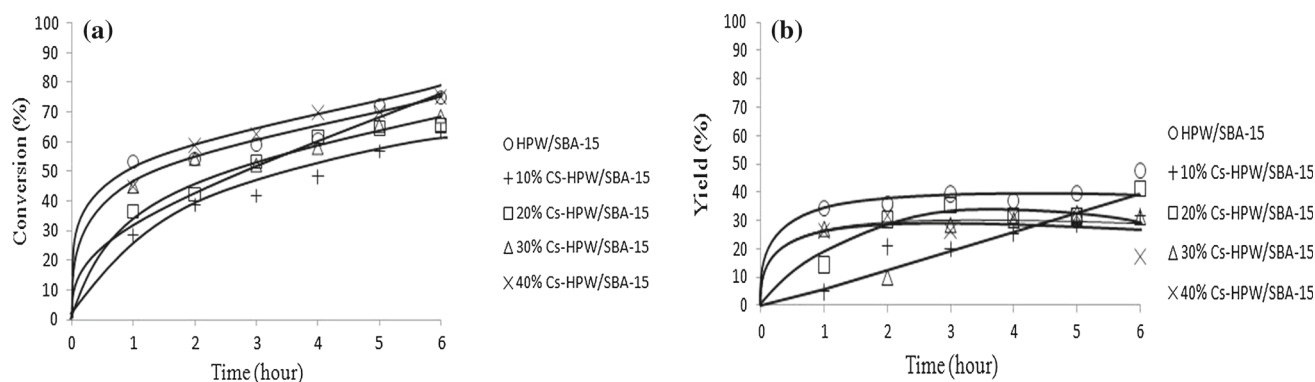


Fig. 6 Effects of Cs-HPW loadings on **a** lauric acid conversion and **b** monolaurin yield (Reaction temperature = 160 °C, reaction time = 6 h, catalyst loading = 2.5 wt%, glycerol/lauric acid = 4:1)

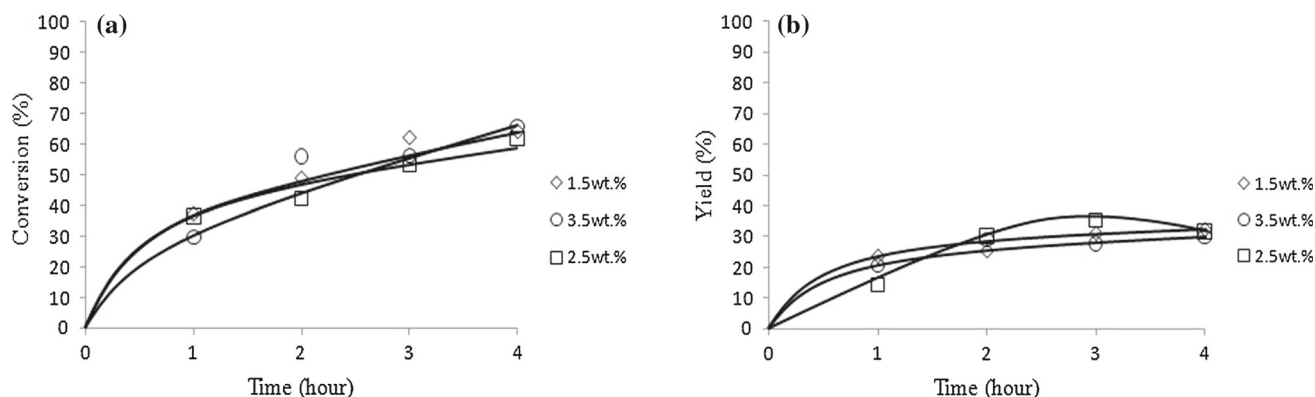


Fig. 7 Effects of catalyst loading on **a** lauric acid conversion and **b** monolaurin yield for 20 wt% Cs-HPW/SBA-15 (Reaction temperature = 160 °C, reaction time = 4 h, glycerol/lauric acid = 4:1)

less vacant or available mesopores. The crystals and deposits on the catalyst's external surface might cause difficulty for the active acid sites to be accessed during the reaction, especially after few hours of reaction. This finding is consistent with the results obtained from the SEM and EDX analyses in Fig. 4 and Table 3, respectively.

Figure 6b shows the monolaurin yield obtained after 6 h of reaction. It was observed that higher catalyst loading (30 and 40 wt%) gave higher yields at the beginning of the reaction (0 to 1 h) but after 2 h, 20 wt%Cs-HPW/SBA-15 catalyst showed the highest yield (41.3%). Although the 40 wt% catalyst might have the highest conversion, but it was not selective toward monolaurin. Therefore, in this study, 20 wt%Cs-HPW/SBA-15 was chosen as the best catalyst to give high monolaurin yield. Furthermore, the equilibrium conversion was achieved after 3 h of reaction and the increment of the yield for the next hours of reaction was significantly low. Hence, it would be more economical to shorten the reaction time to 4 h.

3.2.2 Effect of Catalyst Loading

Effects of catalyst loading (1.5, 2.5 and 3.5 wt%) on the lauric acid conversion and monolaurin yield are shown in Fig. 7. As shown in Fig. 7a, an increase in the catalyst loading from 1.5 to 3.5 wt% increased the lauric acid conversion from 64 to 66%. This is attributed to the increasing number of active acidic sites available to facilitate the reaction. Based on the trend, higher catalyst loading exceeding 3.5 wt% is not favored in this reaction considering the insignificant increase in the conversion after 4 h of reaction. At certain catalyst loading, there will be excess catalyst acidic active sites than required. This would result in no further increment in the conversion even for a prolonged period. Similar finding was also observed using HSO₃SBA-15 catalyst in the reaction involving lauric acid and glycerol [2].

Meanwhile, the monolaurin yield as a function of reaction time is shown in Fig. 7b. The highest monolaurin yield (31.6%) was obtained using 2.5 wt% of catalyst loading and for 3.5 wt% catalyst loading, the monolaurin yield slightly dropped to 30%. Such observation indicated that 2.5 wt% of catalyst loading have had the maximum number of acidic active sites required for the esterification reaction. Further increase in the catalyst loading would result in the formation of bulkier molecules like di- and trilaurin on the external surface of the catalyst that leads to the lower monolaurin yield. From the results in Fig. 7b, there was actually not much difference in the yield for all catalysts. The difference between those catalysts was less than 1%. Hence, the effect of catalyst loading could actually be considered as insignificant. Still, the best catalyst loading to yield high activity for this particular reaction was 2.5 wt% with respect to the limiting reactant.

3.2.3 Effect of Reaction Temperature

Effects of reaction temperature (150, 160 and 170 °C) on the lauric acid conversion and monolaurin yield were investigated and are shown in Fig. 8. This study was conducted at a glycerol/lauric acid of 4, reaction time of 4 h using 2.5 wt% of 20 wt%Cs-HPW/SBA-15 catalyst. In this study, the continuous removal of water from the reaction mixture successfully shifted the equilibrium toward the glycerides formation beyond the thermodynamic equilibrium. As a result, higher conversion of lauric acid was achieved. An increase in the reaction temperature from 150 to 170 °C significantly increased the conversion from 46.2 to 71.8%. This finding is consistent with the fact that for an endothermic reaction, the equilibrium conversion generally increases with temperature. This is caused by the high molecular velocities of the bulky molecules at elevated temperature which consequently increases the entropy [27]. At high reaction temperature, the reactant molecules have adequate energy to overcome the energy barrier resulting in accelerated rate of reaction. Furthermore, the kinetic energy is higher to result in the rapid mass transfer of the bulky molecules within the porous channels. As a result, the number of chemisorption on the active sites will be enhanced. Meanwhile at low temperature of 150 °C, low activity was observed at the beginning of reaction. At this temperature, the possibility of effective collision was low due to the lower energy possessed by the reactant molecules [5]. Since both of the kinetic and potential energies are low at this temperature, the activation energy needed for the conversion of lauric acid would be harder to overcome. As for the other temperatures (160 and 170 °C), the conversion was almost similar after 1 h of reaction.

Figure 8b shows the yield of monolaurin as a function of reaction time. As shown in the figure, the yield of monolaurin obtained after 2 h at 150 °C was the lowest. This might be attributed to the formation of other by-products like di- and trilaurin. Meanwhile, an increase in the temperature by 10 °C resulted in a significance increase in the monolaurin yield. The yield at 170 °C was found to be 44.9%, which was notably higher than that of 160 °C (31.6%) and 150 °C (28.4%). Since the glycerol esterification is a highly endothermic reaction, higher temperature would improve the extent of esterification. Based on the conversion and yield trends, it can be concluded that the reaction temperature of 170 °C was the best temperature in this study.

3.2.4 Effect of Glycerol-to-Lauric Acid Ratio

The effect of glycerol-to-lauric acid molar ratio (2:1–4:1) on the lauric acid conversion and monolaurin yield is shown in Fig. 9. The result in Fig. 9a shows that the increase in the molar ratio increased the reaction rate to consequently improve the lauric acid conversion. This could be explained

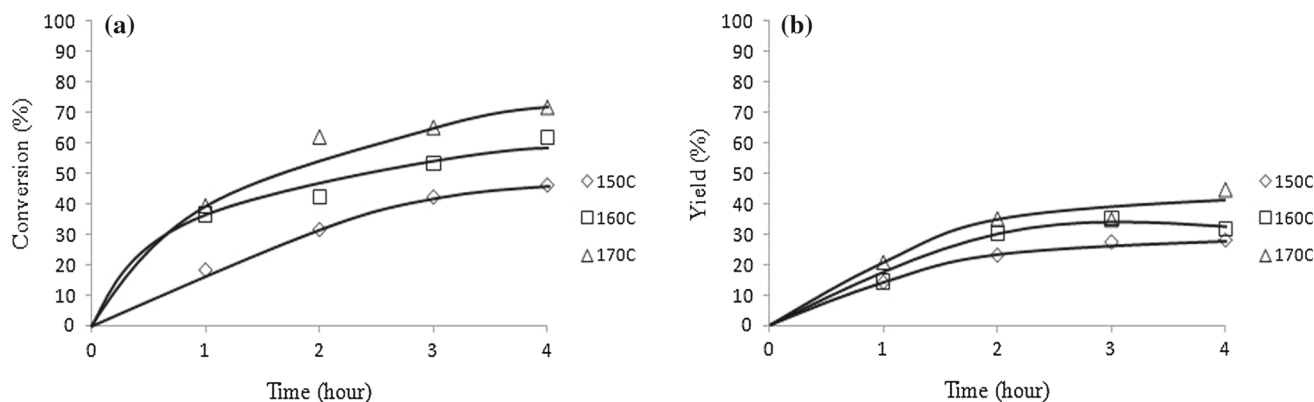


Fig. 8 Effects of reaction temperature on **a** conversion **b** monolaurin yield shown by 20 wt%Cs-HPW/SBA-15 at different reaction temperatures (Catalyst loading = 2.5 wt%, reaction time = 4 h, glycerol/lauric acid = 4:1)

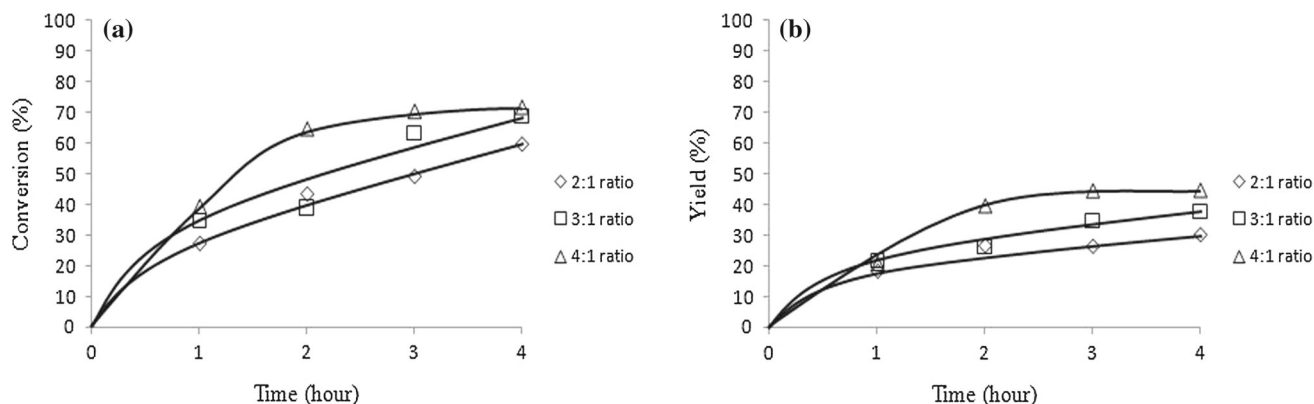


Fig. 9 Profiles of **a** conversion **b** monolaurin yield shown by 20 wt%Cs-HPW/SBA-15 at different reactant ratios (Reaction temperature = 170°C, catalyst loading = 2.5 wt%, reaction time = 4 h, glycerol/lauric acid = 4:1)

based on the fact that in an excess of glycerol, high amount of glycerol was available to allow the reaction with lauric acid molecules to produce mono-, di- and trilaurin. However, the increase in the lauric acid conversion was insignificant when the molar ratio was increased from 3:1 to 4:1 at 4 h of reaction. Although an increase in the glycerol amount is favorable to ensure the forward reaction to form products, the effects were found to diminish beyond a certain amount. This was attributed to the dilution of the limiting reactant (lauric acid) which brought an adverse effect on the lauric acid conversion [28]. Although the highest reaction rate was observed for molar ratio of 4, the high reactant ratio only benefited in the early hours of reaction. This was when the reactants were at high concentrations which increased the chance for lauric acid to react with glycerol mainly in the pores of Cs-HPW/SBA-15 catalysts. As the conversion proceeded, the glycerol concentration dropped while the lauric acid concentration was way too low to proceed toward the forward reaction. In addition, an excess of glycerol probably covered the active sites in the catalyst which prevented the adsorption of lauric acid. Nevertheless, the increase in the conversion was only significant at the beginning of the

reaction. Toward the end of the reaction, the conversions for the molar ratio of 3 and 4 were almost similar which were around 69–72%.

Figure 9b shows the yield of monolaurin at different molar ratios. It was observed that molar ratios influenced the yield of monolaurin. The yield increased from 30.3 to 44.9% when the molar ratios were increased from 2:1 to 4:1. This was attributed to the high amount of glycerol available which increased the possibility for lauric acid to react with glycerol within the mesoporous channels [2]. Therefore, the earlier attached molecules like monolaurin that diffused out from the internal pores would not further react with lauric acid to form di- and trilaurin. This consequently increased the concentration of monolaurin in the reaction mixture. However, no significant change in the yield was observed for the molar ratio of 4 after 3 h of reaction. As the reaction prolonged, the yield was found to be maintained at around 44%. This result suggests that the selectivity of monolaurin did not increase at molar ratios higher than 4, but the formation of di- and trilaurin increased instead. A similar observation was reported on the esterification of glycerol with lauric acid in the presence of HSO₃SBA-15 [29] and HPA supported on SBA-15 cat-

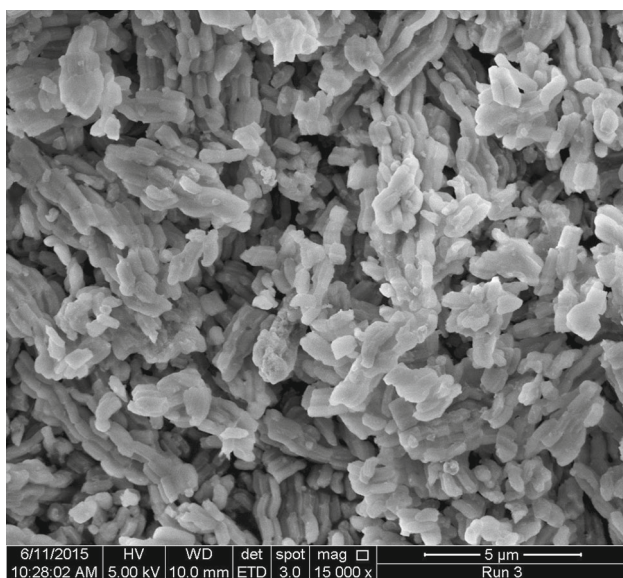


Fig. 10 SEM images of 20 wt%Cs-HPW/SBA-15 catalyst after 3 cycles of reaction

alyst [5]. Therefore, it could be concluded that the reactant ratio affected the initial reaction rate but did not have much effect on the final monoglyceride selectivity.

3.2.5 Stability Study of the Catalyst

The 20 wt%Cs-HPW/SBA-15 catalyst was tested in the esterification reaction to demonstrate the stability of the catalyst in terms of the morphological and chemical properties. After each reaction, the catalyst was recovered and centrifuged to separate the catalyst from the liquid mixture. The remaining solid was then washed with toluene and acetone for several times and dried in an oven at 100 °C. Figure 10 shows the SEM image of the catalyst after 3 consecutive runs. There was no significant difference in the morphology compared to the fresh catalyst (as shown in Fig. 4d). Furthermore, no additional crystals or deposits on the catalyst surface were observed after multiple runs to indicate the stability of the catalyst.

Meanwhile, Table 4 shows the EDX analysis results for both of the fresh and the spent catalyst after 3 consecutive cycles. The results indicated that Cs-HPW/SBA-15 catalyst was suitable to be reused in this reaction. The reduction in the total catalyst loading was around 4.8 wt% which was reasonably low after 3 consecutive cycles. This proved that the catalyst did not undergo very much leaching after each cycle. The presence of P and W elements in the product mixture could be considered insignificant because the total reduction in catalyst loading after 3 cycles of reaction was very low. This brings into a conclusion that the leaching of the active sites from the support was minimal to cause the homogeneous reaction. Therefore, it could be

Table 4 EDX analysis of the fresh 20 wt%Cs-HPW/SBA-15 and the spent catalyst

Catalyst	Component				
	O (wt%)	Si (wt%)	W (wt%)	Cs (wt%)	S (wt%)
Fresh	50.90	30.70	17.04	1.35	0.00
Spent	64.89	20.10	11.87	1.73	1.18

concluded that the 20 wt%Cs-HPW/SBA-15 catalyst played a vital role as a heterogeneous catalyst which showed rather good catalytic activity in several cycles of reactions without experiencing severe deactivation. Since two-sequential-step post-impregnation method was employed in this work, the catalyst might have formed covalent bonding between the Cs-HPW to the mesoporous silica matrix. Hence, the effect of pore blockage or leaching would be reduced significantly. Apart from being an insoluble salt (Cs salt of HPW on SBA-15 support), the covalent bond between the active sites with the support was also proven to play a vital role in preventing leaching [30]. Having these two properties, the catalyst used in this work could be assured to be very stable and almost no leaching of any elements from the solid catalyst would occur; hence, no further testing was actually required.

However, a slight decrease in the total weight of Si and W elements were observed after three cycles of reaction to suggest that minor deactivation could have occurred. This might be due to the deactivation of the acidic active sites or defects in some of the mesopores in the SBA-15. The decrease in the Si element indicated that the mesoporous structure of the silica was slightly destructed while the decrease in the W element suggested that WO_3 that was originally present on the external surfaces of the catalyst was diminished. Interestingly, the amount of Cs slightly increased from 1.35 to 1.73 wt% after a few cycles. This might be due to the Cs elements from the internal pores that diffused out from the internal surface to the outer surface which in turn increased the amount of available active sites. Hence, the reaction rate would be increased despite the reduced activity of the catalyst after several runs.

Furthermore, this catalyst showed rather good activity with only 2% loss in its activity after three consecutive runs compared to the other reported HPA supported SBA-15 catalysts. It was previously reported that phosphotungstic acid loaded on pure SBA-15 showed severe HPW leaching in alcohol oxidation reaction with H_2O_2 [31]. In another study, phosphotungstic acid loaded on hydrophilic ionic liquid modified SBA-15 also displayed the obvious loss of activity in further recycles [32]. Besides, 1.2 wt% of sulfur (S) element was also detected after being reused for three cycles. This could be attributed to the strong chemisorption of the catalyst's active sites with the traces of S impurities which

was simultaneously produced in the gaseous phase during the reaction at high temperature. Although this catalyst showed minor S poisoning, the effect was not detrimental to conclude that the 20 wt%Cs-HPW/SBA-15 catalyst was a stable catalyst which could be reused without severe deactivation of the active sites and its catalytic activity.

4 Conclusions

The esterification of glycerol with lauric acid over different loading of Cs-HPW/SBA-15 catalysts was successfully investigated. The increase in the Cs-HPW loadings increased the immobilization of active phase on SBA-15 and improved the activity toward high lauric acid conversion and monolaurin yield. Based on the correlation between the catalyst characteristics and its activity, it was found that 20 wt%Cs-HPW/SBA-15 catalyst was the best catalyst for this particular reaction in which it required shorter reaction time (4 h) to obtain 71.8% of lauric acid conversion with 44.9% of monolaurin yield. The highest monolaurin yield was achieved at a temperature of 170 °C using a glycerol-to-lauric acid ratio of 4 and 2.5 wt% of catalyst loading. Furthermore, this catalyst was morphologically stable and reusable for up to 3 cycles during the esterification reaction without any significant deactivation and loss of its activity.

Acknowledgements A Research University Grant (814181) and a Dana Inovasi Awal Grant (AUPI00234) from Universiti Sains Malaysia and a Transdisciplinary Research Grant Scheme (6762001) from the Ministry of Higher Education Malaysia are gratefully acknowledged.

References

1. Yusoff, M.H.M.; Abdullah, A.Z.: Catalytic behavior of sulfated zirconia supported on SBA-15 as catalyst in selective glycerol esterification with palmitic acid to monopalmitin. *J. Taiwan Inst. Chem. Eng.* **60**, 199–204 (2016)
2. Hermida, L.; Abdullah, A.Z.; Mohamed, A.R.: Synthesis of monoglyceride through glycerol esterification with lauric acid over propyl sulfonic acid post-synthesis functionalized SBA-15 mesoporous catalyst. *Chem. Eng. J.* **174**, 668–676 (2011)
3. Alrouh, F.; Karam, A.; Alshaghel, A.; El-Kadri, S.: Direct esterification of olive-pomace oil using mesoporous silica supported sulfonic acids. *Arab. J. Chem.* **10**(1), S281–S286 (2017)
4. Simsek, V.; Degirmenci, L.; Murtezaoglu, K.: Synthesis of a silicotungstic acid SBA-15 catalyst for selective monoglyceride production. *React. Kinet. Mech. Catal.* **117**, 773–788 (2016)
5. Hoo, P.Y.; Abdullah, A.Z.: Direct synthesis of mesoporous 12-tungstophosphoric acid SBA-15 catalyst for selective esterification of glycerol and lauric acid to monolaurate. *Chem. Eng. J.* **250**, 274–287 (2014)
6. Dias, J.A.; Caliman, E.; Dias, S.C.L.: Effects of cesium ion exchange on acidity of 12-tungstophosphoric acid. *Microporous Mesoporous Mater.* **76**, 221–232 (2004)
7. Rao, P.M.; Landau, M.V.; Wolfson, A.; Shapira-Tchelet, A.M.; Herskowitz, M.: Cesium salt of a heteropolyacid in nanotubular channels and on the external surface of SBA-15 crystals: preparation and performance as acidic catalysts. *Microporous Mesoporous Mater.* **80**, 43–55 (2005)
8. Landau, M.V.; Rao, P.M.; Thomas, S.; Pitchon, V.; Zukerman, R.; Vradman, L.; Herskowitz, M.: Application of Cs salt of 12-tungstophosphoric acid supported on SBA-15 mesoporous silica in NO_x storage. *Top. Catal.* **42**, 203–207 (2007)
9. Ibrahim, S.M.; El-Shobaky, G.A.: Catalytic efficiency of cesium and potassium salts of dodecatungstophosphoric acid supported on silica and comparison with H3PW12O40/SiO₂. *Kinet. Catal.* **49**, 484–492 (2008)
10. Chiou, J.; Liu, S.; Ho, K.; Huang, H.; Tang, C.; Wang, C.: Camodified Co/SBA-15 catalysts for hydrogen production through ethanol steam reforming. *Int. Lett. Chem. Phys. Astron.* **5**, 1–16 (2014)
11. Gagea, B.C.; Lorgouilloux, Y.; Altintas, Y.; Jacobs, P.A.; Martens, J.A.: Bifunctional conversion of n-decane over HPW heteropoly acid incorporated into SBA-15 during synthesis. *J. Catal.* **265**, 99–108 (2009)
12. Niiyama, H.; Saito, Y.; Echigoya, E.: In: Proceedings, 7th International Congress on Catalysis, Tokyo, 1980. Kodansha, Tokyo/Elsevier, Amsterdam (1981)
13. Gallegos-Suarez, E.; Pérez-Cadenas, M.; Guerrero-Ruiz, A.; Rodriguez-Ramos, I.; Arcoya, A.: Effect of the functional groups of carbon on the surface and catalytic properties of Ru/C catalysts for hydrogenolysis of glycerol. *Appl. Surf. Sci.* **287**, 108–116 (2013)
14. Ertl, G.; Knözinger, H.; Weitkamp, J.: Preparation of solid catalysts. Wiley, New York (2008)
15. Khder, A.E.R.S.; Hassan, H.M.A.; El-Shall, M.S.: Acid catalyzed organic transformations by heteropoly tungstophosphoric acid supported on MCM-41. *Appl. Catal. A Gen.* **411–412**, 77–86 (2012)
16. Olutoye, M.A.; Wong, S.W.; Chin, L.H.; Amani, H.; Asif, M.; Hameed, B.H.: Synthesis of fatty acid methyl esters via the transesterification of waste cooking oil by methanol with a barium-modified montmorillonite K10 catalyst. *Renew. Energy* **86**, 392–398 (2016)
17. Ravikovitch, P.I.; Neimark, A.V.: Experimental confirmation of different mechanisms of evaporation from ink-bottle type pores: Equilibrium, pore blocking, and cavitation. *Langmuir* **18**, 9830–9837 (2002)
18. Van Der Voort, P.; Ravikovitch, P.I.; De Jong, K.P.; Benjelloun, M.; Van Bavel, E.; Janssen, A.H.; Neimark, A.V.; Weckhuysen, B.M.; Vansant, E.F.: A new templated ordered structure with combined micro- and mesopores and internal silica nanocapsules. *J. Phys. Chem. B* **106**, 5873–5877 (2002)
19. Rao-Ginjupalli, S.; Mugawar, S.; Rajan, N.P.; Balla, P.K.; Komandur, V.R.C.: Vapour phase dehydration of glycerol to acrolein over tungstated zirconia catalysts. *Appl. Surf. Science* **309**, 153–159 (2014)
20. Qiao, S.Z.; Bhatia, S.K.; Zhao, X.S.: Prediction of multilayer adsorption and capillary condensation phenomena in cylindrical mesopores. *Microporous Mesoporous Mater.* **65**, 287–298 (2003)
21. Chen, Y.; Zhang, X.-L.; Chen, X.; Dong, B.-B.; Zheng, X.-C.: MCM-41 supported 12-tungstophosphoric acid mesoporous materials: preparation, characterization, and catalytic activities for benzaldehyde oxidation with H₂O₂. *Solid State Sci.* **24**, 21–25 (2013)
22. Pistonesi, C.; Juan, A.; Irigoyen, B.; Amadeo, N.: Theoretical and experimental study of methane steam reforming reactions over nickel catalyst. *Appl. Surf. Sci.* **253**, 4427–4437 (2007)
23. Zhao, D.; Feng, J.; Huo, Q.; Melosh, N.; Fredrickson, G.H.; Chmelka, B.F.; Stucky, G.D.: Triblock copolymer syntheses of mesoporous silica with periodic 50 to 300 Angstrom pores. *Science* **279**, 548–552 (1998)
24. Liu, S.; Wang, X.; Wang, K.; Lv, R.; Xu, Y.: ZnO/ZnS-PdS core/shell nanorods: synthesis, characterization and application for



- photocatalytic hydrogen production from a glycerol/water solution. *Appl. Surf. Sci.* **283**, 732–739 (2013)
25. Amani, H.; Ahmad, Z.; Hameed, B.H.: Highly active alumina-supported Cs-Zr mixed oxide catalysts for low-temperature transesterification of waste cooking oil. *Appl. Catal. A Gen.* **487**, 16–25 (2014)
 26. Junior, L.; da Silva, O.; Cavalcanti, R.M.; Matos, T.M.; Angelica, R.S.; da Rocha Filho, G.N.; Barros, IdCL: Esterification of oleic acid using 12-tungstophosphoric supported in flint kaolin of the Amazonia. *Fuel* **108**, 604–611 (2013)
 27. Dange, P.N.; Rathod, V.K.: Equilibrium and thermodynamic parameters for heterogeneous esterification of butyric acid with methanol under microwave irradiation. *Resour. Effic. Technol.* **3**, 64–70 (2017)
 28. Hashemizadeh, I.; Abdullah, A.Z.: Influence of process conditions on glycerol esterification catalyzed by tetra-n-butylammonium-modified montmorillonite catalyst. *Online J. Sci. Technol.* **2**, 47–51 (2012)
 29. Hermida, L.; Abdullah, A.; Mohamed, A.: Effects of functionalization conditions of sulfonic acid grafted SBA-15 on catalytic activity in the esterification of glycerol to monoglyceride: a factorial design approach. *J. Porous. Mater.* **19**, 835–846 (2012)
 30. Abouzari-Iotf, E.; Nasef, M.M.; Zakeri, M.; Ahmad, A.; Ripin, A.: Composite membranes based on heteropolyacids and their applications in fuel cells. In: Inamuddin, D., Mohammad, A., Asiri, A.M. (eds.) *Organic-Inorganic Composite Polymer Electrolyte Membranes: Preparation, Properties, and Fuel Cell Applications*, pp. 99–131. Springer, Cham (2017)
 31. Macierzanka, A.; Szeląg, H.: Esterification kinetics of glycerol with fatty acids in the presence of zinc carboxylates? Preparation of modified acylglycerol emulsifiers. *Ind. Eng. Chem. Res.* **43**, 7744–7753 (2004)
 32. Palani, A.; Pandurangan, A.: Esterification of acetic acid over mesoporous Al-MCM-41 molecular sieves. *J. Mol. Catal. A Chem.* **226**, 129–134 (2005)

